Water-Soluble Photoinitiators from Dimethylamino-Substituted Monoacylphosphine Oxide for Hydrogel and Latex Preparation

Héloïse Thérien-aubin, Cuong Minh, Quoc Le, Tatiana Petitory, Xingyu Wu, Arnaud Spangenberg, Joanna Ortyl, Mariusz Galek, Lorena Infante, Héloïse Thérien-Aubin, et al.

Water-soluble photoinitiators from dimethylamino-substituted monoacylphosphine oxide for hydrogel and latex preparation

Cuong Minh Quoc Le, Tatiana Petitory, Xingyu Wu, Arnaud Spangenberg, Joanna Ortyl,[*]

Mariusz Galek, Lorena Infante, Héloïse Thérien-Aubin, and Abraham Chemtob[*]

* To whom correspondence should be addressed: abraham.chemtob@uha.fr (+33 3 8960 8834) or jortyl@pk.edu.pl.

C. M. Q. Le, T. Petithory, X. Wu, Dr. A. Spangenberg, Dr. A. Chemtob
Université de Haute-Alsace, CNRS, IS2M UMR7361, F-68100 Mulhouse, France
Université de Strasbourg, France

Dr. J. Ortyl, Prof.
Cracow University of Technology, Faculty of Chemical Engineering and Technology, Warszawska 24, 31-155 Cracow, Poland
Photo HiTech Ltd, Bobrzyńskiego 14, 30-348 Cracow, Poland

Dr. M. Galek
Photo HiTech Ltd, Bobrzyńskiego 14, 30-348 Cracow, Poland

L. Infante, Dr. H. Thérien-Aubin
Max Planck Institute for Polymer Research, Ackermannweg 10, D-55128 Mainz, Germany

Keywords: radical photoinitiator, photopolymerization, water-soluble, phosphine oxide

Abstract

In order to respond to the growing demand for radiation-curable waterborne products like hydrogels or inks, there is a need for water-soluble radical photoinitiators exhibiting absorption in the near UV to visible range. We describe herein the synthesis of a novel type-I diphenylphosphine oxide photoinitiator bearing a 2,6-dimethyl-4-dimethylaminobenzoyl group. The presence of a tertiary amino group in the para position of the benzoyl group results in an increased absorption in the visible range and its facile conversion into water-soluble derivatives after a subsequent protonation or quaternization reaction. Quaternization with methyl triflate (MeOTf) yields a water-soluble monoacylphosphine oxide compound displaying a quaternary ammonium group $-N(CH_3)_3^+$ OTf^-. The main characteristics are water-solubility, shelf-stability, absorption in near-UV range, low cytotoxicity, and efficient α-scission as evidenced by steady-state photolysis experiments. Its photopolymerization efficiency has been evaluated by real-time Fourier transform infrared spectroscopy at 385 and 420 nm using an aqueous solution of poly(ethylene glycol) acrylate. The polymerization rate is comparable to that obtained with the conventional water-soluble monoacylphosphine oxide TPO-Li. Using this new photoinitiator, 3D-printed hydrogels and aqueous polymer dispersions can be prepared.

1. Introduction

Several distinct advantages drive the development of photopolymerization in academic research compared to thermal polymerization: spatial control, formulation photolatency, possibility to turn on and off the polymerization, and high initiation rates. Photopolymerization is also applied industrially with specific process conditions, involving typically solvent-free systems and multifunctional reagents to produce cross-linked films from 100% solids formulations. Inks, overprint varnishes, photoresists, composites, and industrial coatings are thus produced by photopolymerization with economic and environmental advantages.[1, 2] In all cases, a photoinitiator (PI) is one of the key components to control the polymerization efficiency and the properties of the final polymer product.[3] Today the overwhelming majority of radical PIs are oil-soluble because the solvent-free formulations employed industrially require the PI to be soluble in a mixture of monomers and oligomers (mostly oil-soluble).[4]

However, the photopolymerization landscape is changing with the emergence of new processes and products requesting a broader portfolio of water-soluble PIs. For example, 3D-printed hydrogels for biomedical applications,[5] waterborne UV-LED inkjet inks,[6] or waterborne colloidal dispersions[7] have raised a demand for water-soluble PIs. To date, only a limited range of water-soluble PIs have been reported in the literature; among them, very few are available commercially. Irgacure 2959 (1-[4-(2-hydroxyethoxy)-phenyl]-2-hydroxy-2-methyl-1-propanone) is the most used water-soluble type-I PI due to its commercial availability for many years. However, this hydroxyacetophenone derivative suffers from a limited water-solubility (< 1.5% w) and a weak absorption at longer wavelengths up to 360 nm (ε_{365} = 4 M^{-1} cm^{-1}).[8, 9] Two main synthetic pathways have been reported to improve the solubility of the PIs in aqueous

media.[10] First, a physical approach in which oil-in-water microemulsions containing an oil-soluble PI were spray-dried to form a water-dispersible powder.[11] Second, the chemical modification of well-established and efficient oil-soluble acylphosphine oxide type-I PIs such as 2,4,6-trimethylbenzoyl-diphenylphosphine oxide (**TPO**) or bisacylphosphine oxide (**BAPO**) (see chemical structures in **Figure 1**). Following this approach, a poly(ethylene oxide)-substituted BAPO was synthesized (**PEG-BAPO**)[12, 13] as well as various alkali earth metal salts of phosphonic acid (**TPO-Li**, **TPO-Na, BAPO-ONa**, **BAPO-OLi**).[8, 9, 14] These PIs have a higher water-solubility than Irgacure 2959, and a weak absorption band in the UVA-vis around 350-420 nm. Host-guest chemical interaction involving cyclodextrin and conventional hydrophobic initiators represent another attractive route to water-soluble photoinitiatiators.[15-16] Recently, water-soluble type-II PIs were also described using bisphosphonic acid- and bisphosphonate-functionalized benzophenone and thioxanthone PIs.[17, 18] However, this second class of PI has received less attention because their initiating efficiencies are usually lower than the type-I homologs.[10] The concept of water-soluble photoinitiators in general was more comprehensively described in a recent publication.[19] A general comment is that novel efficient water-soluble PIs with enhanced absorption in the near UV to visible range (typically from 360 - 420 nm) are desired.[20, 21]

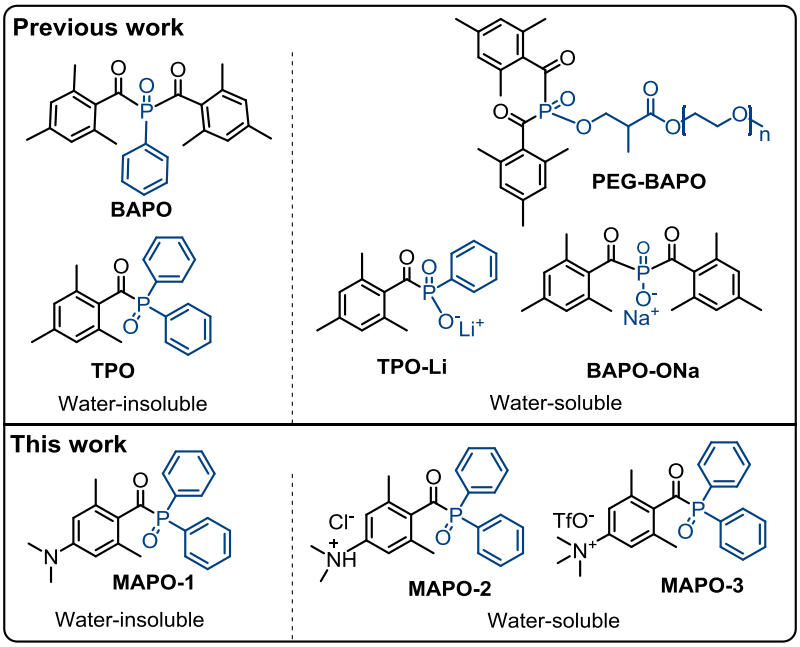

Figure 1. Chemical structures of previously developed water-soluble PIs and their water-insoluble homologues. In this work, the water-insoluble dimethylamino-substituted monoacylphosphine oxide **MAPO-1** was prepared, leading to two water-soluble analogs **MAPO-2** and **MAPO-3**, after protonation or methylation, respectively.

In this study, we describe the synthesis of a novel monoacylphosphine oxide (MAPO) type-I PI bearing a tertiary amino group in the para position of the benzoyl group: (2,6-dimethyl-4-dimethylaminobenzoyl) diphenylphosphine oxide (**MAPO-1**) (**Figure 1**). Compared to **TPO**, the replacement of the mesityl group by a 5-(dimethylamino)-*m*-xylene group results in an increased absorption in the visible range[22-25] and the facile formation of water-soluble derivatives after an additional protonation or quaternization reaction.[26-29] From **MAPO-1**, one can take advantage of the basicity of the amino group to form *in situ* a water-soluble PI (**MAPO-2**) through the terminal protonated amino group $-NH(CH_3)_2^+$ Cl^-. Alternatively, when the PI needs to be isolated, quaternization of **MAPO-1** with methyl triflate (MeOTf) yields a second water-soluble derivative **MAPO-3** bearing a quaternary ammonium group $-N(CH_3)_3^+$ OTf^-. We describe herein

the synthesis of this new family of amino-substituted MAPO compounds. The new PIs are not cytotoxic, present good storage stability, but only the two water-soluble derivatives undergo an efficient α-scission as revealed by steady-state photolysis experiments. The photopolymerization efficiency of **MAPO-3** has been evaluated by real-time Fourier transform infrared spectroscopy (RT-FTIR). Finally, **MAPO-3** has been employed for the 3D printing of hydrogels and synthesis of waterborne polymer dispersions by miniemulsion photopolymerization.

2. Experimental Section

2.1 Chemicals

All reagents were purchased from the chemical providers Sigma Aldrich, TCI, Fluorochem, and Alfa Aesar: 4-bromo-*N*,*N*-dimethylaniline (Sigma Aldrich), Mg for Grignard reactions (99.5%, Sigma Aldrich), dichloro(ethoxy)phosphane (Alfa Aesar), bromobenzene (Alfa Aesar), mesitoyl chloride (Fluorochem), *N*,*N*,3,5-tetramethylaniline (Sigma Aldrich), *N*-bromo succinimide (Fluorochem), trimethylolpropane triacrylate (Across Organics), poly(ethylene glycol) diacrylate (PEGDA, 700 g mol^{-1}, Sigma Aldrich), poly(ethylene glycol) methyl ether acrylate (PEGA, 480 g mol^{-1}, Sigma Aldrich), 3-(trimethoxysilyl)propyl methacrylate (Sigma Aldrich), MnO_2 activated (85%, <10 µm, Sigma Aldrich), methyl trifluoromethane sulfonate (Fluorochem), 3,5-dimethylphenol (Sigma Aldrich), diphenylphosphine oxide (Fluorochem), 2,2'-(ethylenedioxy)diethanethiol (Sigma Aldrich) and trimethylolpropane triacrylate (TCI). These chemicals were used as received without further purification. Dried tetrahydrofuran (THF) for the Grignard reaction was distilled from sodium ketyl and stored with molecular sieves. The reactions were monitored by thin layer chromatography (Silica gel 60 ALUGRAM SIL

G/UV_{254}). The synthesized products were confirmed by liquid chromatography-mass spectrometry (LC-MS) (**Figure S1** in Supporting Information SI) (LCMS-2020 Shimadzu). ^{1}H-NMR and ^{31}P-NMR were recorded in DMSO-d_6, $CDCl_3$ or D_2O on a Varian 300 – NMR.

2.2 Synthesis

Synthesis of 4-(dimethylamino)-2,6-dimethylbenzaldehyde (1). 4-bromo-*N*,*N*,3,5-tetramethylaniline was synthesized according to a modified existing procedure.[30] *N*,*N*,3,5-tetramethylaniline (3.73 g, 25 mmol) was dissolved in 25 mL acetonitrile and then a solution of *N*-bromo succinimide (4.448 g, 25 mmol) in 35 mL acetonitrile was added slowly. The solution was allowed to stir at room temperature (RT) for 110 min. The reaction was quenched with water and extracted three times with hexane. The organic phase was then dried and concentrated. 4-bromo-*N*,*N*,3,5-tetramethylaniline was obtained as a light yellow and clear liquid 5.66 g (yield 97%). ^{1}H NMR (300 MHz, $CDCl_3$) δ 6.51 (s, 2H), 2.91 (s, 6H), 2.38 (s, 6H). A 25 mL Schlenk tube loaded with Mg (0.277 g, 11.4 mmol) and a magnetic stirring bar, was dried with a heat gun for 5 min. When the flask was cooled down to RT, it was refilled with argon. THF (12 mL) was added and followed by the solution of 4-bromo-*N*,*N*,3,5-tetramethylaniline in 2 mL THF (2 g, 8.77 mmol). The solution was then heated to 70^{o}C and stirred at 1000 rpm for 4 hours. The reaction mixture was cooled to RT, and then DMF (1.08 mL, 14 mmol) was added dropwise over 10 min. The reaction was quenched by 10 mL NH_4Cl saturated water and then extracted with 25 mL (× 2) ethyl acetate. The product was obtained by drying and concentrating under vacuum. The raw product was purified by recrystallization in hexane, yielding the off-white solid **1** (1.08 g, yield 69%). ESI(+)MS: [M+H^+] = 178.2 Da. ^{1}H NMR (300 MHz, $CDCl_3$)[31] δ 10.39 (s, 1H), 6.51 (s, 2H), 3.07 (s, 6H), 2.61 (s, 6H).

Synthesis of MAPO-1 and MAPO-2. A 25 mL Schlenk tube loaded with Mg (0.37 g, 15.24 mmol) and a magnetic stirring bar, was dried with a heat gun for 5 min. The tube was cooled down to RT, and then refilled with argon. THF (8 mL) was added, followed by bromobenzene (1.23 mL, 11.7 mmol). The solution was then stirred at RT for 1 h. Subsequently, diethylphosphite (0.5 mL, 3.88 mmol) was added dropwise to the Grignard solution at RT. After 1 h of stirring at RT, the solution was transferred to another Schlenk tube containing **1** (0.76 g, 4.27 mmol) and 2 mL THF and stirred for 1.5 h. The reaction was quenched by combining 10 mL of NH_4Cl saturated aqueous solution. The α-hydroxyphosphine oxide **2** was obtained by multiple extractions to dichloromethane 10 mL (4 ×). **2** was used directly for oxidation without purification. ESI(+)MS: $[M+H^+]$= 380.1 Da. **2** was diluted with 80 mL of dichloromethane, and then activated MnO_2 (6.4 g, 73.7 mmol) was added to a 100 mL round bottom flask. The flask was wrapped with aluminum foil and then stirred at RT for 18 h. The solid catalyst MnO_2 was filtered through a Celite layer. The product was purified by flash chromatography (SiO_2, hexane/ethyl acetate). **MAPO-1** was isolated as a yellow solid 0.15 g (yield over two steps 10%) $[M+H^+]$ = 378.1 Da, $[2M+H^+]$ = 755.2 Da. ^{1}H NMR (300 MHz, $CDCl_3$) δ 8.05 – 7.92 (m, 4H), 7.62 – 7.44 (m, 8H), 3.00 (s, 6H), 2.13 (s, 6H). ^{31}P NMR (121 MHz, $CDCl_3$) δ 13.57. **MAPO-2** was obtained by dissolving **MAPO-1** in a 2 M aqueous HCl solution.

Synthesis of MAPO-3. MAPO-1 (38 mg, 0.1 mmol) was dissolved in 3 mL of Et_2O:CH_2Cl_2 mixture (2:1 v/v) in a 5 mL round bottom flask. Methyl trifluoromethane sulfonate (68 µL, 0.6 mmol) was added dropwise to the flask. After stirring for 10 min, a white precipitate formed and the mixture was continuously stirred for 2 h. The solid product was collected by filtration and washed with 20 mL of Et_2O:CH_2Cl_2 (1:1 v/v). **MAPO-3** was obtained after drying under vacuum

(24 mg, yield 46%) as an off-white solid. [M+H$^+$]=392.1 Da. ^{1}H NMR (300 MHz, DMSO-d_6) δ 7.97 – 7.84 (m, 4H), 7.76 – 7.60 (m, 8H), 3.56 (s, 9H), 2.02 (s, 6H). ^{31}P NMR (121 MHz, DMSO-d_6) δ 13.94

3D printing of polyacrylate hydrogels. Poly(ethylene glycol) diacrylate (M_n = 700 g mol^{-1}, PEGDA 700, 2.0 g) was dissolved in 2.0 mL of water. **MAPO-3** (15.6 mg, 0.8% w/w of PEGDA 700) was added to this aqueous solution. A 3D-DLP printer (Asiga Pico 2 HD 385) equipped with a 385 nm UV LED projector was employed for the preparation of the hydrogel. The printing area was 51.8 mm × 29 mm and consists of 1920 × 1080 pixels, which results in a single-pixel having projected dimensions of 27 μm × 27 μm. The CAD designs of the prints were made with OpenSCAD and exported as STL files. Asiga Composer Software was used to import the STL design file and digitally slice it into a sequence of images that typically contained only black or white pixels. A drop of the formulation was applied onto a glass coverslip pre-treated with 3-(trimethoxysilyl)propyl methacrylate in toluene. After printing, the glass slide with the printed object was developed and rinsed with ethanol.

Synthesis of polymer latex by miniemulsion photopolymerization. An organic phase containing 2,2-(ethylenedioxy)diethanedithiol (1.70 g, 9.2 mmol), diallyl phthalate (2.3 g, 9.2 mmol), 2,5-di-tert-butylhydroquinone (40.5 mg, 50 mM with respect to monomer) and hexadecane (0.16 g, 200 mM with respect to monomer) was mixed in a 25 mL vial. The organic phase was then mixed with 16 mL aqueous phase containing sodium dodecyl sulfate (0.14 g, 3.5% w/w of monomer). The macroemulsion emulsion was initially formed by high-speed mixing with ultra-turax setting at 20 000 rpm for 5 min. The resulting macroemulsion was further emulsified by using a Branson sonifier SFX250 for 5 min at 90% amplitude and pulse

mode 5 s ON / 1 s OFF cycles. A portion of 2 g of miniemulsion was mixed with **MAPO-3** (4 mg, 1% w/w of monomers). 0.5 g of monomer miniemulsion containing the PI was placed in 2 mm optical-thick cuvette and irradiated without stirring for 20 min. See details of the photoreactor and latex characterization in the literature.[32]

2.3 Characterization and methods

UV-vis measurement and steady-state photolysis. Absorption spectra were measured using a SilverNova spectrometer (StellarNet, Inc., Tampa, USA) equipped with a broadband tungsten-deuterium UV-Vis light source (StellarNet, Inc., Tampa, USA). The samples were dissolved in acetonitrile or distilled water and placed in a 1 cm optical path quartz cuvette. For the steady-state photolysis experiment, the solution of PI in acetonitrile (or water) was placed in a cuvette containing a magnetic stirrer and purged with argon for 2 min. The cuvette was irradiated with a UV-LED-385 M385L2 (from Thorlabs Inc.) emitting light at λ_{max} = 385 nm (~600 mW cm^{-2}). The light source was regulated by a DC2200 power supply (from Thorlabs Inc.). The spectra were recorded in real-time during irradiation with a temporal resolution (2 s for the first 150 scans and 5 s for the last 100 scans).

Storage stability. PI was dissolved in distilled water at a concentration of 1 mM in an amber flask. UV-vis spectra of the solution were recorded at t = 0 and after 30 days of storage. The decrease in the percentage of the absorbance at 375 nm of the n-π^* transition was used to evaluate the stability of the PI.

Real-time Fourier-transform infrared spectroscopy. The polymerization kinetics of PEGA in an aqueous solution containing a water-soluble PI was evaluated using an infrared

spectrometer (Thermo Scientific Nicolet iS50). The FTIR was equipped either with a 385 nm LED light guide (LC-L1V3, Hamamatsu, 211 mW cm^{-2}) or a 420 nm LED (M420L3, Thorlabs, 6.0 mW cm^{-2}). The monomer aqueous solution contained PEGA (50% w/w of water) and **MAPO-3** (0.03% w/w of PEGA). The monomer solution was then added to a spectroscopic cuvette (optical thickness of 1 mm) and placed horizontally so as to be irradiated vertically. The IR spectra were recorded every 0.13 s for a total duration of 60 s. For the exposure to 420 nm, the irradiation was prolonged up to 10 min. The polymerization kinetic was determined from the decay of the absorption of acrylate double bond at 6216-6131 cm^{-1} (assigned to two C-H bonds of the vinyl group). The double bond conversion was given by equation 1.

$$Conversion\ (\%) = \left(1 - \frac{A_t}{A_{\ t=0}}\right) \times 100 \quad (1)$$

Photo-DSC measurements.

The photo-DSC studies were conducted with a Photo-DSC 204 F1 Phoenix (Netzsch, Gerätebau GmbH, Germany) equipped with 365, 385, and 405 nm LED light spot cure system (Bluepoint LED eco, UV Technology, Germany). An aqueous solution of PEGA at 50% w/w of water containing **MAPO-3** (1% w/w of PEGA) was irradiated with a LED light source. The irradiance was set at 18.7 mW cm^{-2} irrespective of the irradiation wavelength. The maximum heat of polymerization (t_{max}), the rate of polymerization, and the double bond conversion were calculated.

Cytotoxicity measurements.

The mouse myoblast cell line C2C12 was used for cytotoxicity experiments. The test was performed after 1×10^4 cells (cultured in DMEM (Dulbecco's Modified Eagle's Medium) high

glucose 10% FBS, Fetal Bovine Serum 1% P/S Penicillin/Streptomycin) adhered 24 hours into a plate of 48 wells. The medium was changed by a dilution of PI in medium at 5 different concentrations. After 6 h the colorimetric assays MTT (3–(4,5-dimethylthiazol-2-yl)-2,5-diphenyltetrazolium bromide) was realized. The MTT reagent reacted 4 h with the cells, and then the blue-colored formazan crystals were dissolved in acidic isopropanol. The absorption measurement was made at the UV/Vis spectrophotometer at 570 nm with reference to 620 nm. Measurement uncertainty was determined by means of technical replicates. For this, cytotoxicity the tests were repeated using the same batch of cells and the same PI solution.

3. Results and discussion

3.1 Synthesis of MAPO-1, MAPO-2 and MAPO-3

Acylphosphine oxide derivatives are generally synthesized by two main routes depicted in **Scheme 1**. The first route involves the Michaelis-Arbuzov reaction, in which an acid chloride reacts with an alkoxyphosphine (**route 1**).[33, 34] Developed by Fischer et al.,[35] the second method has been recently the subject of extensive research to synthesize novel α-carbonyl phosphine oxides derivatives (not necessarily soluble in water).[25, 36-40] This latter involves two steps, first, the addition of a secondary phosphine oxide to an aldehyde in the presence of a base catalyst to yield a α-hydroxyphosphine oxide. Subsequent oxidation allows the formation of the desired acylphosphine oxide product (**route 2**). For the synthesis of **MAPO-1**, both routes were investigated using a range of different experimental conditions (see **Scheme S1** and **S2** in SI). The first route did not result in the desired product, while route 2 led to a very limited yield (<

7%) (see details in **Table S1** of SI). Then, we decided to develop a third methodology offering an alternate approach to synthesize the α-hydroxyphosphine oxide intermediate obtained in route 2.

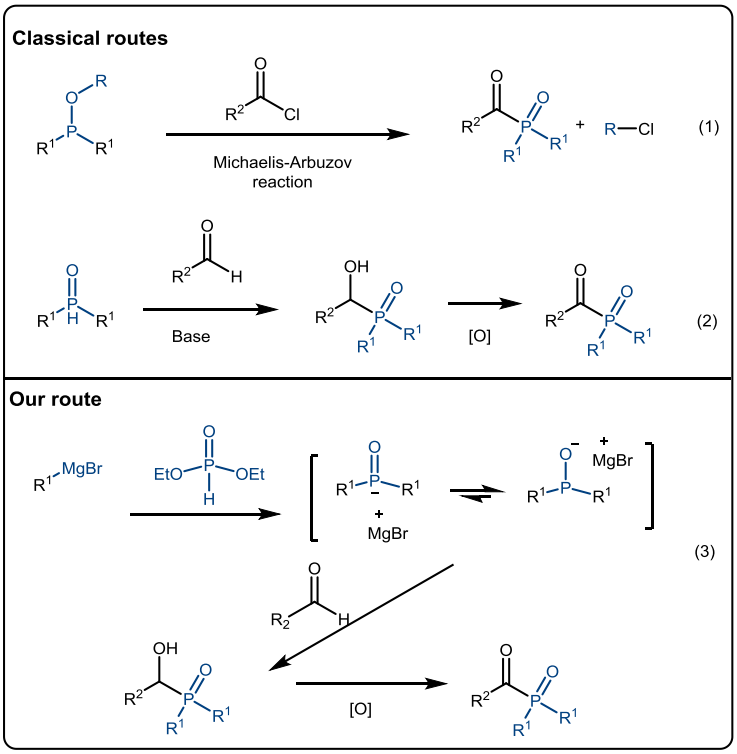

Scheme 1. Two main routes (**1**) and (**2**) for the preparation of acylphosphine oxide derivatives and the newly developed route (**3**) used to synthesize **MAPO-1**.

Scheme 1 shows that in our novel synthetic route (**route 3**), diethylphosphite $(EtO)_2P(=O)H$ reacts with a Grignard reagent R^1MgX and results in the initial deprotonation followed by the displacement of the ethoxy groups to form the intermediate R^1_2POMgX. Further reaction with an aldehyde $R^2C(=O)H$ yields the α-hydroxyphosphine oxide $R^2C(-OH)P(=O)R^1_2$ after hydrolysis. The latter compound is then converted into the desired benzoyl phosphine oxide $R^2C(=O)P(=O)R^1_2$ by oxidation (similarly to the second step of **route 2**).[41] The specific

mechanism for the synthesis of **MAPO-1** is given in **Scheme 2.** Diethylphosphite is reacted with three equivalents of Grignard reagent phenylmagnesium bromide. The expected intermediate $Ph_2POMgBr$ is then added to 4-(dimethylamino)-2,6-dimethylbenzaldehyde (**1**)**.** Hydrolysis with an aqueous ammonium chloride solution yields the α-hydroxyphosphine oxide **2** (R^2-$C(OH)P(=O)Ph_2$ with R^2 = 2,6-dimethyl-4-dimethylaminobenzyl). Oxidation by MnO_2 followed by purification using filtration and flash chromatography gives **MAPO-1** as a yellow powder. The product is chemically stable, but the overall yield is only 10% — a moderate value but significantly higher than that obtained with route 2. The low reactivity can be explained by the decreasing electrophilicity of carbonyl caused by the electron-donating groups in ortho and para of the aromatic ring. Two water-soluble derivatives can be prepared from **MAPO-1**. Firstly, **MAPO-2** is readily obtained by acidification with an aqueous HCl solution at 2 M. Secondly, **MAPO-3** is prepared by methylation with methyl triflate. The **MAPO-3** is isolated as a chemically stable dry powder.

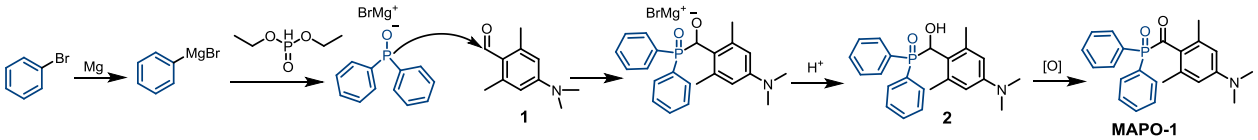

Scheme 2. New route (3) for the synthesis of **MAPO-1**

3.2 Characterization

3.2.1 UV-Vis absorption properties and storage stability

The UV-vis absorption spectra of the three novel PIs in acetonitrile (**MAPO-1)** and water (**MAPO-2**, **MAPO-3**) are shown in **Figure 2**, **TPO** and **TPO-Li** being used as a reference. The

strong electron-donating property of the dimethylamino group in **MAPO-1** increases the energy level of the HOMO orbitals, causing a significant bathochromic shift of the π-π* transition compared to **TPO**.[24] This transition overlaps almost entirely with the typical transition n−π* of **TPO**. However, the π-π* transition blue-shifts when the dimethylamino group is protonated ($NH(CH_3)_2^+$) in **MAPO-2** or methylated in $-N(CH_3)_3^+$ in **MAPO-3**. **MAPO-2** and **MAPO-3** have much lower absorption properties in water compared to their water-insoluble parent **MAPO-1**: 530 M^{-1} cm^{-1} at 365 nm and 140 M^{-1} cm^{-1} at 405 nm (**Table 1**). Nevertheless, these extinction coefficient values are still higher than those of **TPO-Li** (ε_{365} = 218 M^{-1} cm^{-1}) and **Irgacure 2959** (ε_{365} = 4 M^{-1} cm^{-1}).[8] In addition, it is also important to investigate the storage stability of the three PIs in solution (in acetonitrile or water). **MAPO-1** and **MAPO-2** are highly stable in the dark and at ambient temperature without noticeable spectral change. In contrast, **MAPO-3** concentration decreases by 2.5% within 30 days (see **Figure S2** in SI), which is in the same range as for conventional acylphosphine oxide PIs.[9] The presence of sterically hindered groups in the structures of **MAPO** PIs explains their high stability, in particular against hydrolysis for the water-soluble structures **MAPO-2** and **MAPO-3**.[42]

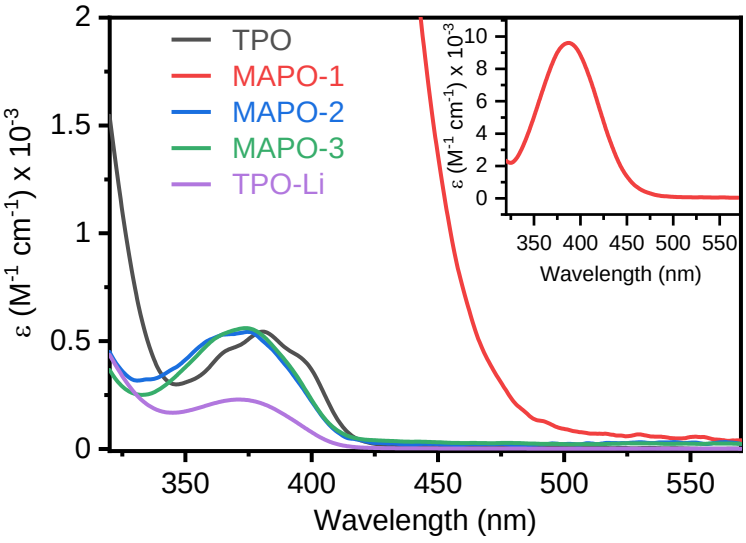

Figure 2. UV absorption spectra of **TPO** and **MAPO-1** in acetonitrile; **MAPO-2** in aqueous HCl 2M, **MAPO-3** and TPO-Li in water. The inset shows the full **MAPO-1** spectrum.

Table 1. Molar extinction coefficients at different wavelengths for conventional PIs (**TPO**, **TPO-Li**) and novel PIs (**MAPO-1**, **-2** and **-3**)

Photoinitiator	**Solvent**	ε (M^{-1} cm^{-1})			
		365 nm	385 nm	405 nm	420 nm
TPO	Acetonitrile	445	521	251	37
MAPO-1		7595	9577	8185	5588
MAPO-2	Aqueous HCl 2 M	530	458	140	40
MAPO-3	Water	530	476	141	40
TPO-Li		218	188	44	6

3.2.2 Steady-state photolysis

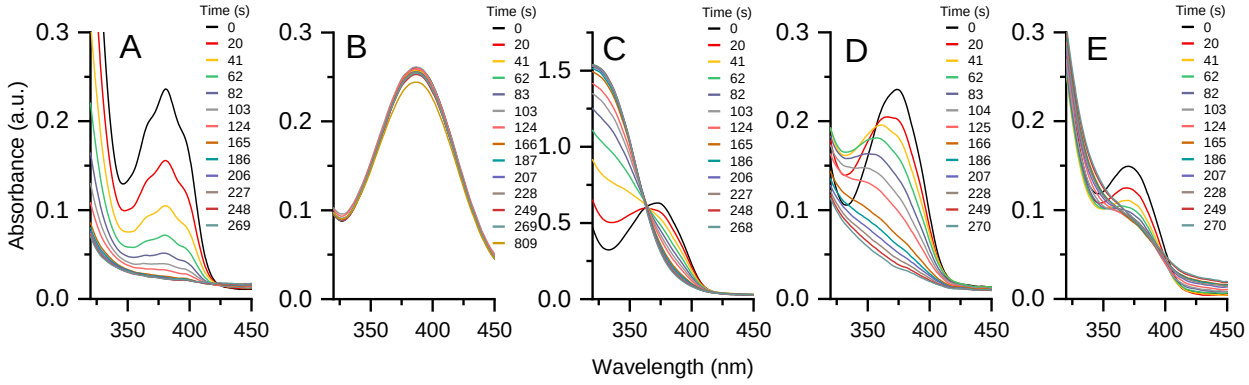

Figure 3. Steady-state photolysis under irradiation at 385 nm (86 mW cm^{-2}) of **TPO** (**A**) and **MAPO-1** (**B**) in acetonitrile; **MAPO-2** in HCl aqueous solution 2 M (**C**); **MAPO-3** (**D**) and **TPO-Li** (**E**) in water.

Figure 3 shows the steady-state photolysis of the new **MAPO** PIs in solution when exposed to irradiation at 385 nm. The photolysis of the water-insoluble **MAPO-1** (**B**) can be reasonably compared with that of **TPO** (**A**). The **MAPO-2** (**C**) and **MAPO-3** (**D**) decomposition are better

compared with that of **TPO-Li** (**E**). In all cases, the maximum absorptions of the π-π* transition gradually decrease with irradiation time, suggesting a PI decomposition. A photolysis ratio *w%* is calculated using equation 2.[43]

$$w\% = \frac{\Delta A}{A_0} = \frac{(A_0 - A_t)}{A_0} \quad (2)$$

Where A_0 is the absorbance at the maximal absorption wavelength before light irradiation, and A_t represents the absorption after an irradiation time *t*. Interestingly, all photoinitiating systems show an absorption decay following a first-order kinetic, described by the equation 3.[43]

$$ln\left(\frac{10^{A}-1}{10^{A_0}-1}\right) = -k \times t \quad (3)$$

Where *k* is the photolysis rate (s^{-1}). Consistently, the plots of $ln\left(\frac{10^{A}-1}{10^{A_0}-1}\right)$ as a function of the irradiation time yield straight lines for the series of PIs (**Figure 4**). The coefficient of determination (R^2) of the plots higher than 0.99 confirms the goodness of fit of the linear model. The photolysis rate of **MAPO-1** is extremely slow, at least two orders of magnitude smaller than that of **TPO**. This slow photolysis rate was attributed to the presence of a dimethylamino group responsible for the red-shift of π-π* transition. The overlapping of the π-π* and n-π* transitions likely hinders the photocleavage of (O=)C-P(=O) bond.[44] Conversely, **MAPO-2** and **MAPO-3** exhibiting a well-defined π-π* transition show a much higher photolysis efficiency. Their photolysis rates are about in the same order of magnitude ($8\ 10^{-3}\ s^{-1}$) as that of **TPO-Li**. These results exemplify the influence of benzoyl substituent on the structure-reactivity of acylphosphine type PI. Furthermore, they also show the potential of **MAPO-2** and **MAPO-3** for performing photopolymerization in aqueous media, as discussed in section 3.3.

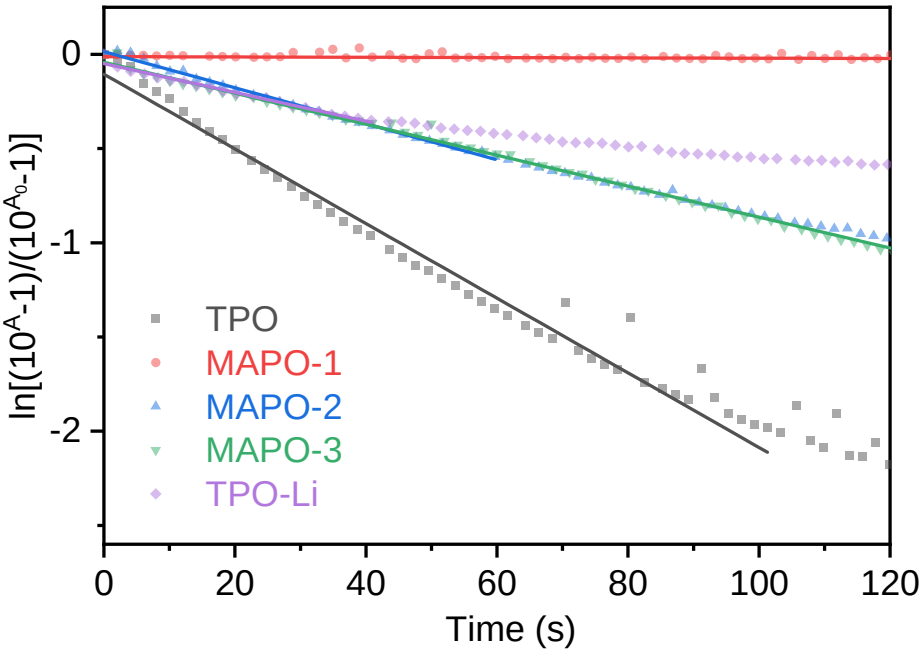

Figure 4. Photolysis rates of various water-insoluble PIs (**TPO**, **MAPO-1**) and water-soluble PIs (**TPO-Li**, **MAPO-2**, **MAPO-3**) when exposed to an irradiation at 385 nm (86 mW cm^{-2}).

3.2.3 Cytotoxicity

Evaluation of the non-cytotoxicity and biocompatibility of the new-water soluble PI **MAPO-3** is an important requirement considering its potential application in biological media or medical devices. *In vitro* cytotoxicity experiments were performed with an MTT assay using myoblasts (cell line C2C12). **Figure 5** shows the cell viability (%) after 6 h of incubation as a function of PI concentration (0.3 - 3.9 mM). The cellular metabolic activity of the samples remains at the same level as the control PI-free sample up to a PI concentration of 1 mM. At the highest concentration of 3.9 mM, only 50% of the metabolic activity is preserved. In contrast, the results show the C2C12 cell cultures are more sensitive to phenol, a well-known cytotoxic species used as a positive control test.

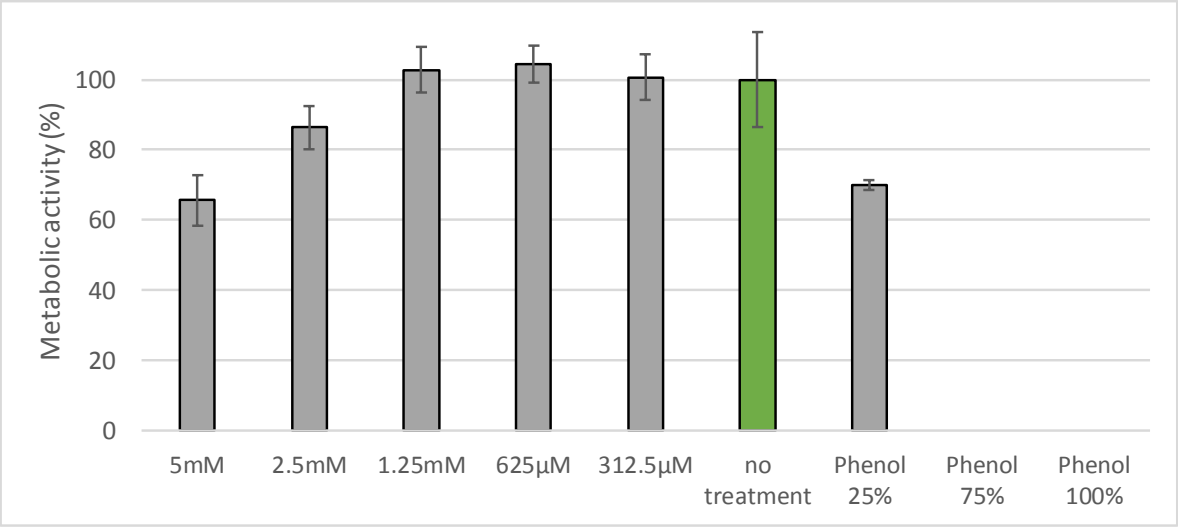

Figure 5. C2C12 cytotoxicity assay of **MAPO-3** aqueous solution at different concentrations. Comparison with a negative (no-treatment) and a positive control (containing phenol solutions).

3.3 Photopolymerization efficiency

3.3.1 RT-FTIR

The reactivity of **MAPO-3** was studied using real-time FTIR, and the results were compared with that obtained with **TPO-Li**. In both cases, the PI was added to an aqueous solution containing 50% w/w of poly(ethylene glycol) methyl ether acrylate (PEGA, 480 g mol^{-1}) to reach a concentration of 0.5 mM (~ 0.03% w/w of monomer). The photopolymerization was performed either at 385 nm or 420 nm. The conversion-time plots for these two irradiation wavelengths are shown in **Figure 6**. At 385 nm (**A**), the double bond conversion of the two PIs proceeds similarly with a fast polymerization rate of 0.7 mol L^{-1} s^{-1}. This result is consistent with the similar photolysis decays of **MAPO-3** and **TPO-Li** (Figure 4). At 420 nm (**B**), the PEGA oligomer also polymerizes at the same rate regardless of the PI despite the increased absorption of **MAPO-3** (ε_{385nm} = 476 M^{-1} cm^{-1}) compared to TPO-Li (ε_{385nm} = 188 M^{-1} cm^{-1}) (**Table 2**). Therefore, the

higher absorption properties of **MAPO-3** do not result in an accelerated photopolymerization process. The overall radical PI efficiency is not only dependent on the efficiency of light absorption. Two other crucial factors must be taken into account, which are presumably more favorable in the case of **TPO-Li**: the efficiency of radical generation (related to the quantum yield of triplet formation and photocleavage) and the reactivity of the radicals generated (i.e., addition constant to the acrylate monomer).[22]

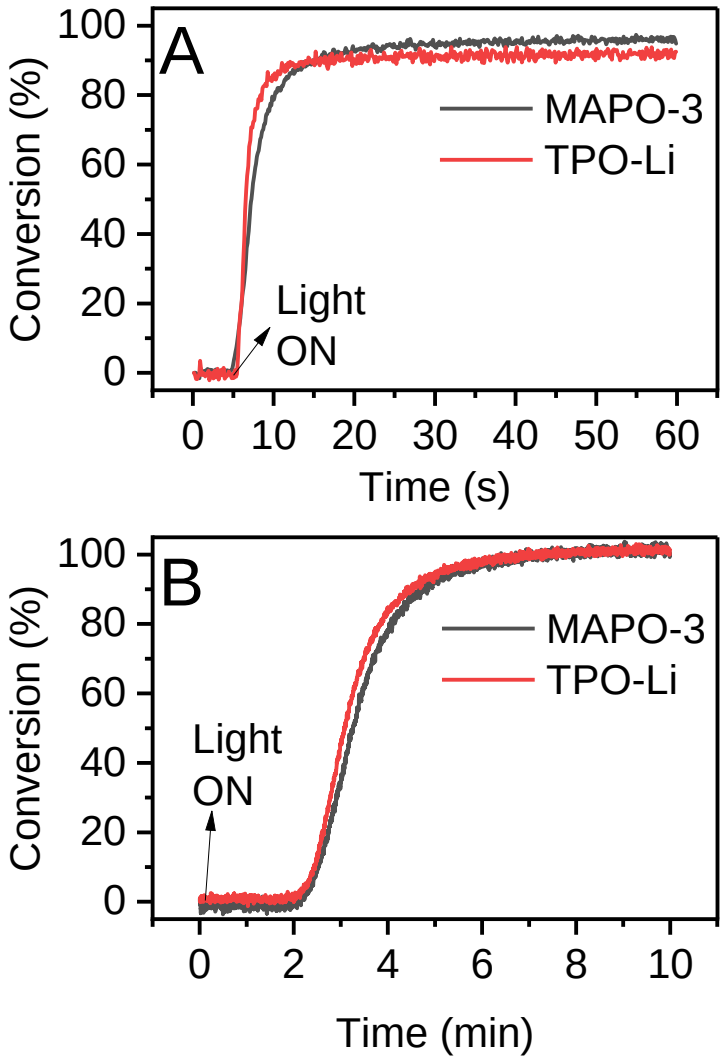

Figure 6. Conversion-irradiation time plot during the photopolymerization of a PEGA aqueous solution (50% w) using **MAPO-3** or **TPO-Li** as water-soluble PI ([PI] = 0.5 mM). The irradiation wavelength is 385 nm (**A**, 211 mW cm^{-2}) and 420 nm (**B**, 6.0 mW cm^{-2}) respectively.

Table 2. FTIR data obtained during photopolymerizations of aqueous PEGA 50% w/w using **TPO-Li** and **MAPO-3** ([PI] = 0.5 mM)

PI	Irradiation wavelength (nm)	ε (M^{-1} cm^{-1})	Induction time (s)	Conversion (%)	R_p (s^{-1})
TPO-Li	385	188	0	94	0.62
	420	6	145	99	0.02
MAPO-3	385	476	0	97	0.61
	420	40	145	99	0.02

3.3.2 Photo-DSC

To investigate further the reactivity of the new PIs, photo-DSC experiments were also carried out using the same oligomer PEGA at similar concentration in water (50% w/w). **Table 3** gathers a series of useful data characterizing the reactivity of **MAPO-3** and **TPO-Li**: t_{max} (s), the time when the maximum heat of polymerization is reached; H_{max} (mW mg^{-1}), the exothermicity of reaction derived from the peak height; R_p (s^{-1}), the polymerization rate; and monomer *conversion* (%) calculated from the heat of polymerization (ΔH). The two PIs show somehow similar behavior (R_p, t_{max}, *Conversion*) for irradiation in the UV range. This supports that **MAPO-3** can be successfully used for photopolymerization processes in aqueous solutions. Interestingly, at 405 nm, the slightly higher extinction coefficient values of **MAPO-3** allow it to achieve significantly higher conversions and polymerization rate than **TPO-Li**. However, the reader is cautioned that FT-IR and DSC data cannot be compared quantitatively, because the polymerizations were carried out under widely different reaction conditions. The main differences between the techniques include film thickness, nature of the atmosphere and irradiation conditions (see experimental section for details).

Table 3. Results of a photopolymerization of a 50% w/w aqueous solution of PEGA containing **MAPO-3** (1% w/w of PEGA) at different irradiation wavelengths: 365, 385, and 405 nm.

PI	Irradiation wavelength (nm)	ΔH (J g^{-1})	t_{max} (s)	H_{max} (mW mg^{-1})	Conversion (%)	$R_p \times 10^2$ [s^{-1}]
TPO-Li	365	83	65.5	11.4	47	6.4
	385	89	66.8	8.1	50	4.5
	405	91	67.7	5.7	51	3.2
MAPO-3	365	95	65.0	9.9	53	5.5
	385	108	66.2	11.1	60	6.2
	405	159	66.1	9.7	89	5.4

3.4 Applications in 3D printing and latex preparation

3.4.1 3D printing of hydrogels

3D printing of polymer hydrogels was conducted under air using **MAPO-3** and an aqueous solution of poly(ethylene glycol) diacrylate (PEGDA, 50% w/w) . The good solubility in water of **MAPO-3** and its high photosensitivity allow for an efficient polymerization process in a commercially available digital light processing 3D printer working at 385 nm. A thick round piece (**Figure 7A)** and the institute logo (**Figure 7B**) can be obtained after a short exposure time (20 s) at 21 mW cm^{-2}. The smooth, high-resolution hydrogel structures demonstrate that this PI is suitable for light-induced additive manufacturing, especially in 3D hydrogel printing. Interestingly, the 3D-printed material loses its yellow color after a few days due to the photobleaching of the residual PI (**Figure 7C**). This post-cure bleaching is well known for white-pigmented formulations and can be accelerated by exposure to daylight and fluorescent lamps.

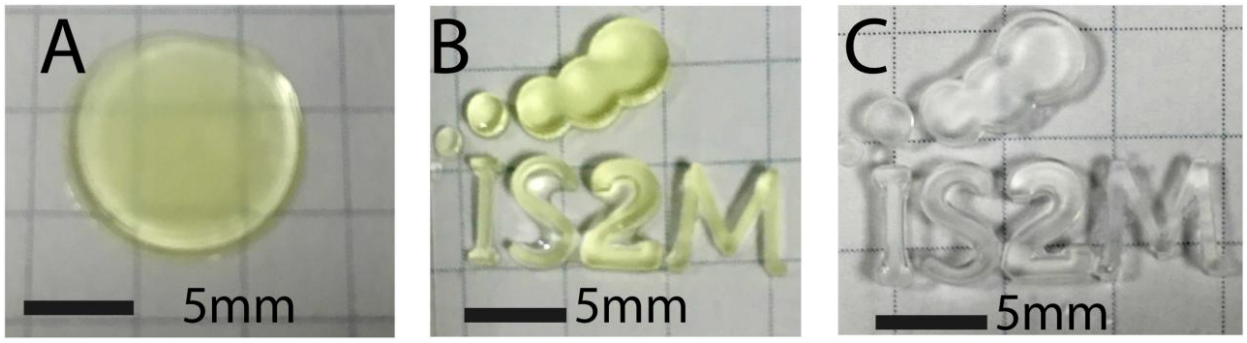

Figure 7. 3D printed hydrogels based prepared from an aqueous solution of PEGDA/water (50% w) using **MAPO-3** (0.8% w/w of PEGDA). Irradiation conditions: 21 mW cm^{-2}, 20 s. (**A**) the round piece, (**B**) IS2M logo, and (**C**) the same 3D-printed object after 3 days.

3.4.2 Preparation of polysulfide latex by thiol-ene miniemulsion polymerization

To broaden the range of polymer products accessible with **MAPO-3**, we also conducted a photopolymerization in an aqueous dispersed system to prepare waterborne polymer colloids. Among the different polymerization processes available, we chose a miniemulsion photopolymerization because it involves small monomer droplets having a lower scattering coefficient than a conventional macroemulsion. In a representative synthesis, an aqueous monomer miniemulsion containing a stoichiometric amount of dithiol monomer (2,2′-(ethylenedioxy)diethanethiol) and diene monomer (diallyl phthalate) was first prepared through a high energy input provided by an ultrasonifier. Coalescence was overcome using surfactant (sodium dodecyl sulfate), while diffusional destabilization was limited by the dissolution of a costabilizer (hexadecane) in the monomer phase. If destabilization phenomena are sufficiently retarded, predominant droplet nucleation may be achieved, and the number of the produced particles is generally in the same range as that of droplets. This mechanism represents the basis of miniemulsion polymerization. In our case, **MAPO-3** (or **TPO-Li**) was added to the thiol-ene

miniemulsion just after preparation (1% w/w of monomers). The miniemulsion was then transferred to a 2 mm optical-thick cuvette and irradiated by a 385 nm light source. The main characteristics of the reaction such as monomer conversion, particle size, and $\overline{M_n}$ and molecular weight dispersity (Đ) are summarized in **Table 4**. Irrespective of the PI employed, a high monomer conversion is achieved, but this latter is slightly lower for the latex prepared from **MAPO-3**. This may explain why significantly lower molecular weights are also obtained in this case. However, ^{1}H NMR spectroscopy supports that the expected poly(thioether) structure is synthesized in both cases. Whatever the PI used, the polymer particles have an intensity-weighted average diameter of approx. 140-150 nm.

Table 4. Effect of PI on latex properties derived from dithiol-diene monomer miniemulsion (thiol:ene = 1:1 equiv.), PI 1% w/ monomer, 20% solids content. Irradiation conditions: 385 nm, 3.1 mW cm^{-2}, 20 min.

PI	Ene conversion (%)[a]	$\overline{M_n}$ (g mol^{-1}) / Đ[b]	Particle diameter (nm) / PDI[c]
TPO-Li	>99	5600 / 2.4	141 / 0.144
MAPO-3	98	2600 / 2.6	147 / 0.101

[a] Determined by ^{1}H NMR in DMSO (**Figure S3** in SI). [b] Determined by gel permeation chromatography (GPC) in THF (**Figure S4** in SI). [c] Z-average diameter or intensity-weighted diameter were determined by dynamic light scattering (DLS). Droplet diameter of monomer miniemulsion was 206 nm (PDI = 0.21). Detailed characterization of the polymer latexes can be found in **Figure S5** in SI.

4. Conclusion

A new approach to synthesizing water-soluble ammonium salts of benzoyl (diphenyl)phosphine oxide is described. A three-step synthesis involving the initial reaction of diethyl phosphite with a diphenyl Grignard reagent, makes it possible to obtain a phosphine oxide containing a 4-dimethylamino-2,6-dimethylbenzoyl structure (**MAPO-1**), but only with a limited yield (10%). Ortho-substitution of the aryl carbonyl group by methyl groups ensures the

solvolytic stability while the para-substitution by dimethylamino drives a strong red-shift of the π-π* transition. In addition, the para-substituted -$N(CH_3)_2$ group makes possible the preparation of two water-soluble PI derivatives via protonation ($NH(CH_3)_2^+$, **MAPO-2**) or methylation (-$N(CH_3)_3^+$, **MAPO-3**). Unfortunately, the two resulting ammonium salts have a much weaker absorption in the long wavelength region (ε_{405nm} = 141 M^{-1} cm^{-1}) than their water-insoluble parent ($\varepsilon_{405nm} = 8.2 \times 10^3$ M^{-1} cm^{-1}) but were around 3 times higher that of TPO-Li (ε_{405nm} = 44 M^{-1} cm^{-1}). Only the water-soluble derivatives can undergo a fast and efficient type-I scission process as proved by steady-state photolysis, but the nature of radical formed was not investigated. A RT-FTIR study proves that **MAPO-3** can be used as PI since it promotes the radical photopolymerization of acrylate aqueous solutions with polymerization rates comparable to those of TPO-Li. **MAPO-3** shows a good storage stability even when it is dissolved in water, and no cytotoxicity is observed below a threshold concentration of 1 mM. **MAPO-3** was successfully involved in the 3D printing of hydrogel or the synthesis of polymer latexes. Considering the potential of this new family of acylphosphine oxide family with dimethylamino-substituted benzoyl group, it is of interest to find more efficient synthetic routes.

Conflicts of interest

There are no conflicts to declare.

Acknowledgements

This project has received funding from the European Union's Horizon 2020 research and innovation programme under the Marie Skłodowska-curie grant agreement n° 765341 (project photo-emulsion, MSCA-ITN-2017). The authors also thank Dr. Jean-Luc Birbaum (retired scientist at BASF-Schweiz) for his valuable help in the discussion of the experimental results.

References

[1] A. B. Scranton, C. N. Bowman, R. W. Peiffer, "*Photopolymerization: fundamentals and applications"*, ACS Publications, New Orleans, Louisiana, 1997.

[2] A. Bagheri, J. Y. Jin, *ACS Applied Polym. Mater.* **2019**, *1*, 593.

[3] J.-P. Fouassier, J. Lalevée, "*Photoinitiators for polymer synthesis: scope, reactivity, and efficiency"*, John Wiley & Sons, Weinheim, Germany, 2012.

[4] J. Lalevée, J. P. Fouassier, "*Photopolymerisation Initiating Systems"*, Royal Society of Chemistry, Cambridge, 2018.

[5] C. Yu, J. Schimelman, P. Wang, K. L. Miller, X. Ma, S. You, J. Guan, B. Sun, W. Zhu, S. Chen, *Chem. Rev.* **2020**, *120*, 10695.

[6] K. Dietliker, J. Baro, "Photoinitiators", in *Handbook of Industrial Inkjet Printing*, W. Zapka, Ed., 2017, p. 59.

[7] F. Jasinski, P. B. Zetterlund, A. M. Braun, A. Chemtob, *Prog. Polym. Sci.* **2018**, *84*, 47.

[8] B. D. Fairbanks, M. P. Schwartz, C. N. Bowman, K. S. Anseth, *Biomaterials* **2009**, *30*, 6702.

[9] S. Benedikt, J. Wang, M. Markovic, N. Moszner, K. Dietliker, A. Ovsianikov, H. Grutzmacher, R. Liska, *J. Polym. Sci. Polym. Chem.* **2016**, *54*, 473.

[10] K. Dietliker, "Chapter 13. Water-soluble Photoinitiators: Present and Future", in *Photopolymerisation Initiating Systems*, The Royal Society of Chemistry, Cambridge, UK, 2018, p. 358.

[11] A. A. Pawar, G. Saada, I. Cooperstein, L. Larush, J. A. Jackman, S. R. Tabaei, N. J. Cho, S. Magdassi, *Sci. Adv.* **2016**, *2*, e1501381.

[12] G. Ullrich, B. Ganster, U. Salz, N. Moszner, R. Liska, *J Polym Sci Polym Chem* **2006**, *44*, 1686.

[13] J. Wang, S. Stanic, A. A. Altun, M. Schwentenwein, K. Dietliker, L. Jin, J. Stampfl, S. Baudis, R. Liska, H. Grutzmacher, *Chem. Commun.* **2018**, *54*, 920.

[14] A. Henne, A. Hesse, M. Jacobi, G. Wallbillich, B. Bronstert (BASF Aktiengesellschaft), US4719297A, **1988**.

[15] N. Zivic, J. Zhang, D. Bardelang, F. Dumur, P. Xiao, T. Jet, D.-L. Versace, C. Dietlin, F. Morlet-Savary, B. Graff, J. P. Fouassier, D. Gigmes and J. Lalevée, *Polym. Chem.* **2015**, *7*, 418.

[16] D. K. Balta, E. Bagdatli, N. Arsu, N. Ocal, Y. Yagci, *J. Photochem. Photobio. A: Chem.* **2008**, *196*, 33.

[17] T. N. Eren, J. Lalevée, D. Avci, *Macromol. Chem. Phys.* **2019**, *220*.

[18] T. N. Eren, T. Gencoglu, M. Abdallah, J. Lalevee, D. Avci, *Eur. Polym. J.* **2020**, *135*.

[19] W. Tomal, J. Ortyl, *Polymers* **2020**, *12*, 1073.

[20] T. V. Holland, F. Chang, R. Desousa (Novartis AG), US 10,324,311 B2, **2019**.

[21] J. Kirschner, J. Paillard, B. Graff, J. M. Becht, J. E. Klee, J. Lalevée, *Macromol. Chem. Phys.* **2020**, *221*.

[22] W. A. Green, "*Industrial photoinitiators: a technical guide"*, CRC Press, Boca Raton, Florida, 2010.

[23] E. Frick, C. Schweigert, B. B. Noble, H. A. Ernst, A. Lauer, Y. Liang, D. Voll, M. L. Coote, A.-N. Unterreiner, C. Barner-Kowollik, *Macromolecules* **2015**, *49*, 80.

[24] J. Radebner, M. Leypold, A. Eibel, J. Maier, L. Schuh, A. Torvisco, R. Fischer, N. Moszner, G. Gescheidt, H. Stueger, M. Haas, *Organometallics* **2017**, *36*, 3624.

[25] C. B. Xie, Z. M. Wang, Y. Y. Liu, L. Song, L. Liu, Z. W. Wang, Q. Yu, *Prog. Org. Coat.* **2019**, *135*, 34.

[26] T. Hayakawa, K. Horie, *Dent. Mater.* **1992**, *8*, 351.

[27] S. Knaus, H. F. Gruber, *J. Macromol. Sci. Pure Appl. Chem.* **1996**, *33*, 869.

[28] S. Dadashi-Silab, C. Aydogan, Y. Yagci, *Polym. Chem.* **2015**, *6*, 6595.

[29] K. Yokoi, H. Tsuyama (Fujifilm Corporation), US 20180362558A1, **2018**.

[30] E. Zysman-Colman, K. Arias, J. S. Siegel, *Can. J. Chem.* **2009**, *87*, 440.

[31] J. Killoran, J. F. Gallagher, P. V. Murphy, D. F. O'Shea, *New J. Chem.* **2005**, *29*, 1258.

[32] C. M. Quoc Le, M. Schmutz, A. Chemtob, *Macromolecules* **2020**, *53*, 2369.

[33] W. Rutsch, K. Dietliker, R. G. Hall (Ciba-Geigy Corporation), US5,218,009, **1993**.

[34] K. Ikemura, K. Ichizawa, M. Yoshida, S. Ito, T. Endo, *Dent. Mater. J.* **2008**, *27*, 765.

[35] M. Fischer, E. Hickmann, R. Kropp, J. Schroeder, B. Trentmann (BASF Aktiengesellschaft), US5679863A, **1997**.

[36] R. Nazir, P. Danilevicius, D. Gray, M. Farsari, D. T. Gryko, *Macromolecules* **2013**, *46*, 7239.

[37] C. Dietlin, T. T. Trinh, S. Schweizer, B. Graff, F. Morlet-Savary, P. A. Noirot, J. Lalevee, *Macromolecules* **2019**, *52*, 7886.

[38] Y. Y. Liu, T. T. Wang, C. B. Xie, X. J. Tian, L. Song, L. Liu, Z. W. Wang, Q. Yu, *Prog. Org. Coat.* **2020**, *142*.

[39] C. Dietlin, T. T. Trinh, S. Schweizer, B. Graff, F. Morlet-Savary, P. A. Noirot, J. Lalevée, *Molecules* **2020**, *25*.

[40] L. Breloy, C. Negrell, A. S. Mora, W. S. J. Li, V. Brezova, S. Caillol, D. L. Versace, *Eur. Polym. J.* **2020**, *132*.

[41] H. R. Hays, *J. Org. Chem.* **1968**, *33*, 3690.

[42] J. Baxter, R. Davidson, H. Hageman, G. Hakvoort, T. Overeem, *Polymer* **1988**, *29*, 1575.

[43] K. Kostrzewska, J. Ortyl, R. Dobosz, J. Kabatc, *Polym. Chem.* **2017**, *8*, 3464.

[44] B. Ganster, U. K. Fischer, N. Moszner, R. Liska, *Macromolecules* **2008**, *41*, 2394.

Table of contents entry

Water-soluble Photoinitiators from Dimethylamino-substituted Monoacylphosphine Oxide for Hydrogel and Latex Preparation

Cuong Minh Quoc Le, Tatiana Petithory, Xingyu Wu, Arnaud Spangenberg, Joanna Ortyl, Mariusz Galek, Lorena Infante, Héloïse Thérien-Aubin, and Abraham Chemtob**

We present an approach to synthesizing new water-soluble radical photoinitiators based on ammonium salts of benzoyl (diphenyl)phosphine oxide.